Automatic detection and correction algorithms for magnetic saturation in the SMFT/HSOS longitudinal magnetograms

Hai-Qing Xu (徐海清)[1][*], Suo Liu (刘锁)[1], Jiang-Tao Su (苏江涛)[1,2][*], Yuan-Yong Deng (邓元勇)[1,2], Andrei Plotnikov[3], Xian-Yong Bai (白先勇)[1,2], Jie Chen (陈洁)[1], Xiao Yang (杨潇)[1], Jing-Jing Guo (郭晶晶)[1], Xiao-Fan Wang (王晓帆)[1] and Yong-Liang Song (宋永亮)[1]

[1] Key Laboratory of Solar Activity, National Astronomical Observatories, Chinese Academy of Sciences, Beijing 100101, China; *xhq@bao.ac.cn, sjt@bao.ac.cn*

[2] School of Astronomy and Space Sciences, University of Chinese Academy of Sciences, Beijing 100049, China

[3] Crimean Astrophysical Observatory, Russian Academy of Sciences, Nauchny, Crimea, 298409, Russia

Abstract A longitudinal magnetic field often suffers the saturation effect in a strong magnetic field region when the measurement is performed at a single-wavelength point and linear calibration is adopted. In this study, we develop a method that can judge the threshold of saturation in Stokes V/I observed by the Solar Magnetic Field Telescope (SMFT) and correct it automatically. The procedure is to first perform the second-order polynomial fit to the Stokes V/I vs. I/I_m (I_m is the maximum value of Stokes I) curve to estimate the threshold of saturation, then reconstruct Stokes V/I in a strong field region to correct for saturation. The algorithm is demonstrated to be effective by comparing with the magnetograms obtained by the Helioseismic and Magnetic Imager (HMI). The accuracy rate of detection and correction for saturation is ∼99.4% and ∼88% respectively among 175 active regions. The advantages and disadvantages of the algorithm are discussed.

Key words: Sun: sunspots — Sun: magnetic field — Methods: data analysis

1 INTRODUCTION

Study of the solar magnetic field has always been a core topic in solar physics. Some major unsolved scientific problems in the study of solar physics, such as generation of the solar cycle, coronal heating, the origin of solar eruptions and so on, are all related to the solar magnetic field. The magnetic field of sunspots was first investigated by Hale (1908). It is known that generally currently operating magnetographs measure solar polarized light (present as Stokes parameters I, Q, U and V) rather than magnetic fields. Under certain atmospheric models and assumptions, the solar magnetic field is obtained through inversion according to radiation transfer theory. The solar magnetic field has been observed for more than a century and many interesting results have been presented from these observations. Yet, there are still some basic questions on the measurements of solar magnetic fields waiting

to be carefully analyzed (Zhang 2019). Svalgaard et al. (1978) found the magnetograph was saturated when the magnetic field is very strong. Ulrich et al. (2002) discussed reasons and treatment of saturation effects in the Mount Wilson 150 foot tower telescope system in detail. They pointed out that most spectral lines utilized for magnetic measurements are subject to this saturation effect for at least some parts of their profile. Liu et al. (2007) found another type of saturation in sunspot umbrae observed by the Michelson Doppler Imager on the Solar and Heliospheric Observatory (MDI/SOHO) caused by the 15-bit onboard numerical treatment used in deriving the MDI magnetograms. The saturation effect can be eliminated by considering information on the spectral line, e.g., the Spectro-Polarimeter (SP) onboard Hinode (Kosugi et al. 2007) obtains the spectral profile with a wide spectral range, and the Helioseismic and Magnetic Imager onboard the Solar Dynamics Observatory (HMI/SDO, Schou et al. 2012) obtains a spectral profile with six

---

★ Corresponding authors

wavelength points. The saturation effect needs to be corrected by some supplementary methods if the polarized light is measured in a single-wavelength point and linear calibration is adopted. Chae et al. (2007) performed cross-calibration of Narrow-band Filter Imager (NFI) Stokes V/I and longitudinal magnetic field acquired by the SP, and proposed utilizing two different linear relationships of longitudinal magnetic field and Stokes V/I from Hinode/NFI to correct for saturation. Moon et al. (2007) used a pair of MDI intensity and magnetogram data simultaneously observed, and the relationship from the cross-comparison between the SP and MDI flux densities to correct for saturation in magnetic field obtained by MDI. Guo et al. (2020) explored a nonlinear calibration method to deal with the saturation problem, which relied on a multilayer perceptron network.

The Solar Magnetic Field Telescope (SMFT) at Huairou Solar Observing Station (HSOS) of National Astronomical Observatories, Chinese Academy of Sciences is a 35 cm vacuum telescope equipped with a birefringent filter for wavelength selection and KD*P crystals to modulate polarization signals. The Fe I 5324.19 Å line is used for measurements. A vector magnetogram is built utilizing four narrow-band (0.125 Å) Stokes I, Q, U and V maps. The center wavelength of the filter can be tuned and is normally at -0.075 Å for the measurements of longitudinal magnetic fields and at the line center for the transverse magnetic fields (Ai & Hu 1986). It has been observing vector magnetic fields for more than 30 years. The theoretical calibration for SMFT vector magnetogram was first made by Ai et al. (1982). Several different methods of the magnetic field calibration under the weak-field assumption have been done since then. Wang et al. (1996) employed an empirical calibration and a velocity calibration method to calibrate the longitudinal magnetograms. Su & Zhang (2004) considered 31 points of the FeI 5324.19 Å spectral line profile to derive vector magnetic field by the non-linear least squares fitting technique. Bai et al. (2014) improved the calibration process by fitting the observed full Stokes information using six points of the profile of the Fe I 5324.19 Å line, and the analytical Stokes profiles under the Milne-Eddington atmosphere model, adopting the Levenberg-Marquardt least-squares fitting algorithm. However, the routine measurements of Stokes I, Q, U and V parameters by SMFT are being performed at a single-wavelength point. The longitudinal magnetic field is reconstructed by Equation (1)

$$B_L^{\mathrm{SMFT}} = C_L \frac{V}{I}, \qquad (1)$$

where C_L is the calibration coefficient inferred from the aforementioned calibration methods. This linear calibration will result in saturation when the magnetic field is strong. Plotnikov et al. (2019) made an attempt to improve the routine magnetic field measurements of SMFT by introducing a non-linear relationship between the Stokes V/I and longitudinal magnetic field. They performed cross-calibration of SMFT data and magnetograms provided by HMI to determine the form of the relationship. They found that the magnetic field saturation inside a sunspot umbra can be eliminated by using the non-linear relationship between Stokes V/I and longitudinal magnetic field. They also discussed the influence of saturation effect on solving the 180 degree ambiguity of the transverse magnetic field. They manually chose the threshold for separating pixels into two subsets of strong and weak magnetic field, which is not convenient for dealing with a large data sample.

In this paper, we attempt to develop a method which can judge the threshold of saturation in SMFT longitudinal field and correct for saturation automatically. One purpose of this study is to correct for saturation in longitudinal magnetic field obtained by SMFT since 1987. Another purpose is to prepare a calibration technique for the Full-disk vector MagnetoGraph (FMG, Deng et al. 2019) which is one payload onboard the Advanced Space-based Solar Observatory (ASO-S, Gan et al. 2019) that will be launched in early 2022. Routine observations for the FMG will be taken at one wavelength position of the Fe I 5324.179 Å (Su et al. 2019). The magnetic field will suffer the saturation effect if linear calibration is adopted.

2 OBSERVATIONS

The raw data registered by SMFT are left and right polarized light. The Stokes V/I and I are calculated as follows

$$\frac{V}{I} = \frac{V_l - V_r}{V_l + V_r},$$
$$I = V_l + V_r, \qquad (2)$$

where $V_l = \frac{I+V}{2}$ and $V_r = \frac{I-V}{2}$ represent modulated filtergrams. After this process, the influence of a flat field is eliminated. The pixel size of SMFT data is approximately $0.29'' \times 0.29''$ since 2012 and the spatial resolution is approximately $2''$ produced by local seeing effect. We select nine active regions (ARs) that were identified between 2013 and 2015 for case study and 175 ARs in 2013 for a statistical study. The data were performed by 4×4 pixel median filtering to reduce the noise.

To check the effectiveness of the correction method for saturation, we downloaded the co-temporal magnetograms

Table 1 Threshold of Detecting Magnetic Saturation for Nine ARs Observed by SMFT

NOAA	Date	Position	I/I_c	I/I_m
11658	2013.01.19	S11W10	0.602	0.497
11899	2013.11.18	N06W03	0.420	0.382
11960	2014.01.25	S14E01	0.661	0.585
12027	2014.04.06	N13W01	0.579	0.492
12055	2014.05.12	N10W02	0.664	0.557
12149	2014.08.27	N10E11	0.543	0.472
12158	2014.09.10	N15E10	0.496	0.444
12305	2015.03.27	S08W04	0.577	0.529
12325	2015.04.19	N04E02	0.638	0.582

of the selected nine ARs from HMI/SDO. HMI is a full-disk filtergraph that measures the profile of photospheric Fe I 6173 Å line at six wavelength positions in two polarization states to derive the longitudinal magnetic field. The spatial resolution of the instrument is $1''$ with $0.5'' \times 0.5''$ pixel size. In order to perform a detailed pixel by pixel comparison, HMI magnetograms are rotated for the *p*-angle correction and reduced in spatial resolution to $2''$ by a 2-D Gaussian smoothing function. Both data are re-scaled to the pixel size of $0.5'' \times 0.5''$. Then the same region that includes the maximized size of sunspots is selected and shifted with respect to each other to determine the optimal registration.

3 METHOD

Studies affirm that there is a relationship between the continuum intensity and magnetic field, and the smallest intensity always corresponds to the largest magnetic field (e.g., Martínez & Vázquez 1993; Norton & Gilman 2004; Leonard & Choudhary 2008). Figure 1(a) and (b) displays the maps of Stokes *I* and *V/I* for AR NOAA 12158 observed on 2014 September 10 by SMFT. Figure 1(c) and (d) features the distribution of Stokes *I* and *V/I* along the red line. The Stokes *I* decreases to its minimum in the sunspot center, but the Stokes *V/I* stops increasing at the points marked by green lines (asterisks) corresponding to sunspot umbrae. This phenomenon is called magnetic saturation. If performing linear calibration, the longitudinal magnetic field will get weakened in sunspot umbrae compared with its surrounding area.

Next, we will showcase two examples to give a detailed description for the detection and correction method for the saturation effect.

3.1 Detection Algorithm for Magnetic Saturation

The relationship between $|V/I|$ and I/I_c (I/I_m) for NOAA 12158 is illustrated in Figure 2(a) ((b)). I_c is

the median value of Stokes *I* within the rectangle region in Figure 1(a). I_m is the maximum value of Stokes *I* within the whole AR. $|V/I|$ first increases with Stokes *I* decreasing (going to sunspot center), then decreases. It is found that the second-order polynomial (red line) gives a good fit when $|V/I| > 0.02$ and $I/I_c \leq 0.8$ ($I/I_m \leq 0.7$). Moon et al. (2007) found a similar relationship between MDI flux density and intensity in magnetic saturation regions, and used a second-order polynomial to separate the strong and weak field area. The pixels are separated into two parts by the apex. It is easy to calculate coordinates of the apex by fitting coefficient. We find that the corresponding I/I_c is 0.496 and I/I_m is 0.444, which are marked in Figure 2(c) and (d) by blue and red contours respectively. Although the values of I/I_c and I/I_m are different, the region in Stokes *I* and $|V/I|$ maps is the same. When $I/I_c < 0.496$ ($I/I_m < 0.444$), it corresponds to the sunspot umbra where the $|V/I|$ suffered from saturation. So, we may regard this value as the threshold to detect the saturation regions in a longitudinal magnetic field.

We performed the same analysis for NOAA 12305 which includes multiple sunspots. We used the observation on 2015 Mar 27. A similar relationship was found between $|V/I|$ and I/I_c (I/I_m) as NOAA 12158 when $|V/I| > 0.02$ and $I/I_c \leq 0.8$ ($I/I_m \leq 0.75$). The I/I_c (I/I_m) is 0.577 (0.529) corresponding to the apex of the second-order polynomial (red line in Fig. 3(a) and (b)), which is represented in Figure 3(c) and (d) by blue and red contours respectively. The region of saturation can also be detected accurately for multiple sunspots.

We listed the thresholds for detecting saturation obtained by the above method for nine ARs in Table 1. It can be seen that the thresholds are different for each AR. So, it is necessary to calculate the threshold for individual ARs. There is no difference in detecting the saturation region utilizing I/I_c and I/I_m, but I/I_m has more advantages than I/I_c in automatic detection.

3.2 Correction Algorithm for Magnetic Saturation

We take the above two ARs as examples to show how to correct the saturation effect. We re-plot $|V/I|$ vs. I/I_m in Figure 4. The correction procedure for magnetic saturation is as follows:
(1) The threshold I_0 for occurrence of magnetic saturation is determined by the above algorithm, which corresponds to green asterisks in Figure 4(a) and (d).
(2) The pixels are separated into two parts by threshold I_0. Those with $I/I_m < I_0$ suffer from the saturation effect. Both linear (green lines in Fig. 4(b) and (e)) and
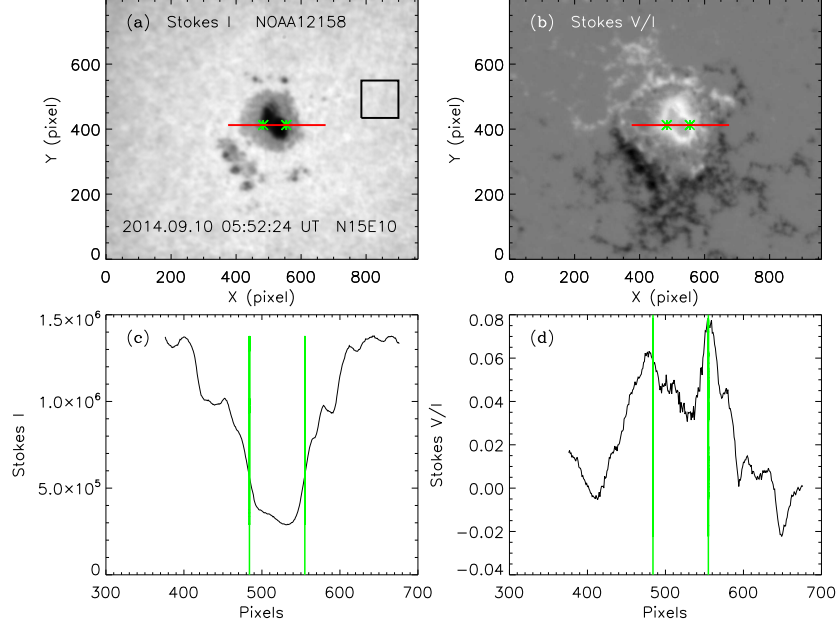
Fig. 1 Panels (a) and (b) are maps of Stokes I and V/I observed on 2014 September 10 by SMFT. The *square region* in panel (a) is used to calculate I_c. Panels (c) and (d) show the distributions of Stokes I and V/I along the *red line*. The *green lines* indicate the saturation locations marked by *asterisks*.

the second-order polynomial functions (yellow lines in Fig. 4(b) and (e)) are used to fit the scatter plots for saturation data. The green and yellow lines almost overlap. For their simplicity, we finally choose the linear functions to fit the scatter plots for both saturation and good data. The fitting coefficients are (a_1, c_1) and (a_2, c_2) corresponding to green and blue lines in Figure 4(b) and (e), respectively. a_1 and a_2 are slopes, c_1 and c_2 are constants. Applying Equation (3) to calculate Stokes V/I for pixels where $I/I_m < I_0$,

$$\frac{V^s}{I} = \left| \frac{a_2}{a_1} \left(\left| \frac{V}{I} \right| - c_1 \right) + c_2 \right| \cdot \text{sign} \left(\frac{V}{I} \right). \quad (3)$$

(3) After re-calculating, the Stokes V/I maps are displayed in Figure 5(a) and (c). It can be seen that the saturation in sunspot umbrae has been eliminated. However, the discontinuity at the boundary of umbrae and penumbrae is visible. To eliminate this discontinuity, we compute the $\pm 1\sigma$ uncertainty of I_0 corresponding to the cyan ($I_{+\sigma}$) and blue ($I_{-\sigma}$) asterisks in Figure 4(a) and (d). For pixels where $I_{-\sigma} < I/I_m < I_{+\sigma}$, V/I is calculated by interpolation, then the data are smoothed by a Gaussian smoothing function. The new V/I maps are featured in Figure 5(b) and (d). It can be ascertained that the discontinuity has been eliminated. The scatter plots of $|V/I|$ vs. I/I_m are depicted in Figure 4(c) and (f). The relationship is approximately linear.

4 COMPARISON BETWEEN SMFT AND HMI DATA

The SMFT longitudinal magnetic field B_L^{SMFT} can be re-calibrated from Equation (4)

$$B_L^{\text{SMFT}} = \begin{cases} C_L \frac{V}{I}^s , & \frac{I}{I_m} < I_0, \\ C_L \frac{V}{I} , & \frac{I}{I_m} \geq I_0, \end{cases} \quad (4)$$

where C_L is the calibration coefficient. We adopt 8381 G as proposed by Su & Zhang (2004).

The comparison between longitudinal magnetic field observed by SMFT and HMI for NOAA 12158 is displayed in Figure 6. It can be seen that the distributions of B_L^{SMFT} and HMI longitudinal magnetic field B_L^{HMI} are very similar (Fig. 6(a) and (b)). The scatter plots of B_L^{SMFT} and B_L^{HMI} before and after correcting saturation effect are shown in Figure 6(c) and (d), respectively. The B_L^{SMFT} starts to decrease when B_L^{HMI} is larger than 1300 G before correcting the saturation effect. The linear correlation coefficient is 0.86. After correcting the saturation effect in B_L^{SMFT}, the relationship of B_L^{SMFT} and B_L^{HMI} is closer to linear. The linear correlation coefficient increases to 0.96. Such good correlation indicates that the proposed correction method for saturation in B_L^{SMFT} is effective for this AR.

Figure 7 shows the comparison of B_L^{SMFT} and B_L^{HMI} for NOAA 12305. It is also found that the B_L^{SMFT} starts
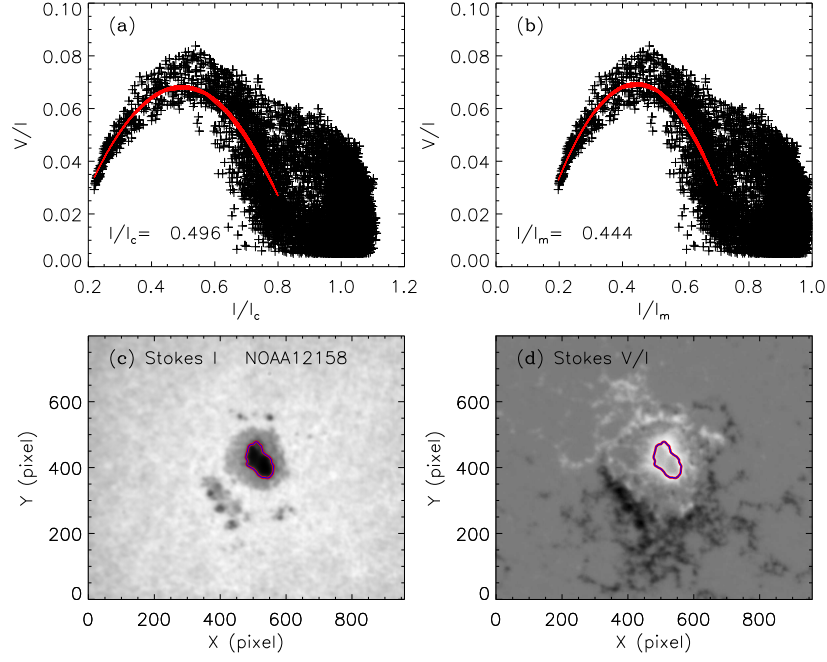
Fig. 2 Scatter plots of $|V/I|$ vs. I/I_c (panel (a)) and I/I_m (panel (b)) for NOAA 12158. The *red line* is the best-fit second-order polynomial and I/I_c (I/I_m) marked in panels (a) and (b) corresponds to the apex. The *red* and *blue contours* in panels (c) and (d) represent I/I_c=0.496 and I/I_m=0.444 respectively. V/I uses the absolute values in the plots, similarly hereinafter.
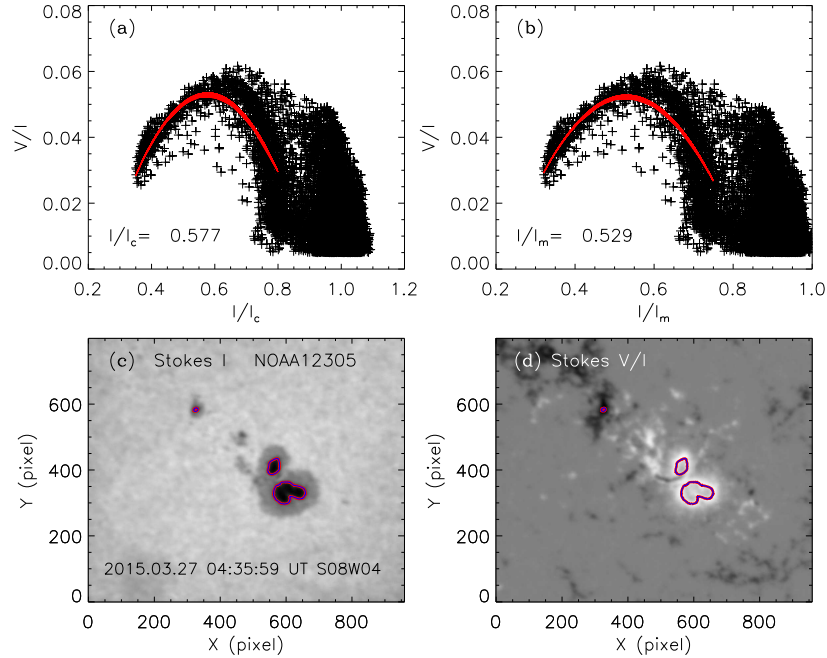

Fig. 3 Similar to Fig. 2, but for NOAA 12305.

to decrease when B_L^{HMI} is larger than 1300 G before correcting the saturation effect. The linear correlation coefficient is 0.88. After correcting the saturation effect in B_L^{SMFT}, a good correlation between B_L^{SMFT} and B_L^{HMI} is found. The linear correlation coefficient increases to 0.96, which indicates that the proposed correction method for saturation in B_L^{SMFT} is also effective for an AR that includes multiple sunspots.
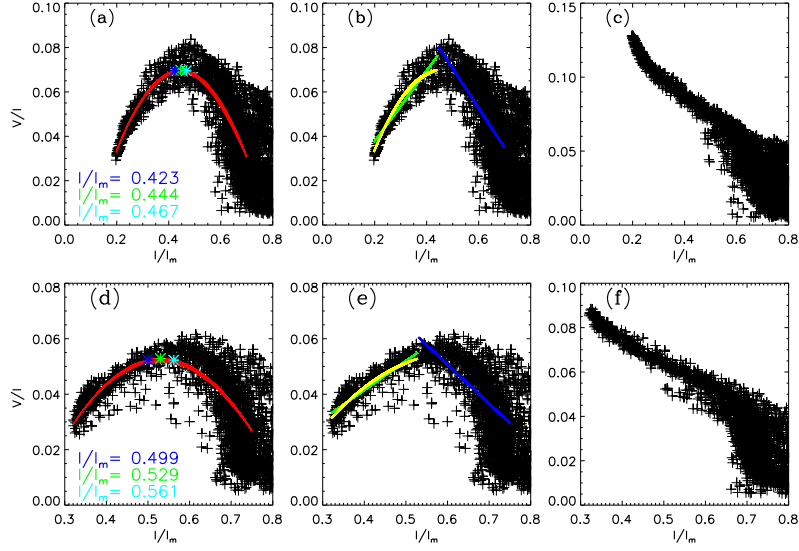
Fig. 4 Scatter plots of $|V/I|$ vs. I/I_m for NOAA 12158 (panels (a)–(c)) and NOAA 12305 (panels (d)–(f)). The *green asterisks* in panels (a) and (d) represent the apex of the second-order polynomial fit (*red line*). The *cyan* and *blue asterisks* indicate the $\pm 1\sigma$ uncertainty of the apex. The corresponding I/I_m values are marked using the same color as those asterisks. The *green* and *blue* (*yellow*) *lines* are the linear (the second-order polynomial) fit to the data in panels (b) and (e). Panels (c) and (f) feature the scatter plots of $|V/I|$ vs. I/I_m after correcting magnetic saturation.
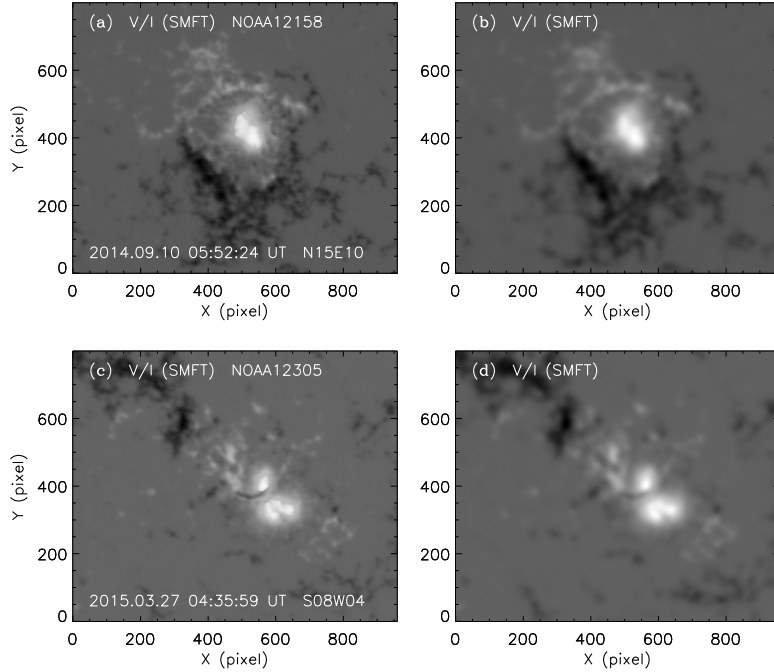

Fig. 5 Maps of Stokes V/I after correcting magnetic saturation for NOAA 12158 (panels (a) and (b)) and NOAA 12305 (panels (c) and (d)). The data in panels (b) and (d) are processed with Gaussian smoothing.

We performed such pixel by pixel comparison for nine ARs and listed the correlation coefficients in Table 2. The correlation of B_L^{SMFT} and B_L^{HMI} is much better after eliminating magnetic saturation in B_L^{SMFT}. So, the detection and correction algorithms can be applied to re-

calibrate the longitudinal magnetic field in the strong field region observed by SMFT.

5 TESTING FOR A LARGE SAMPLE

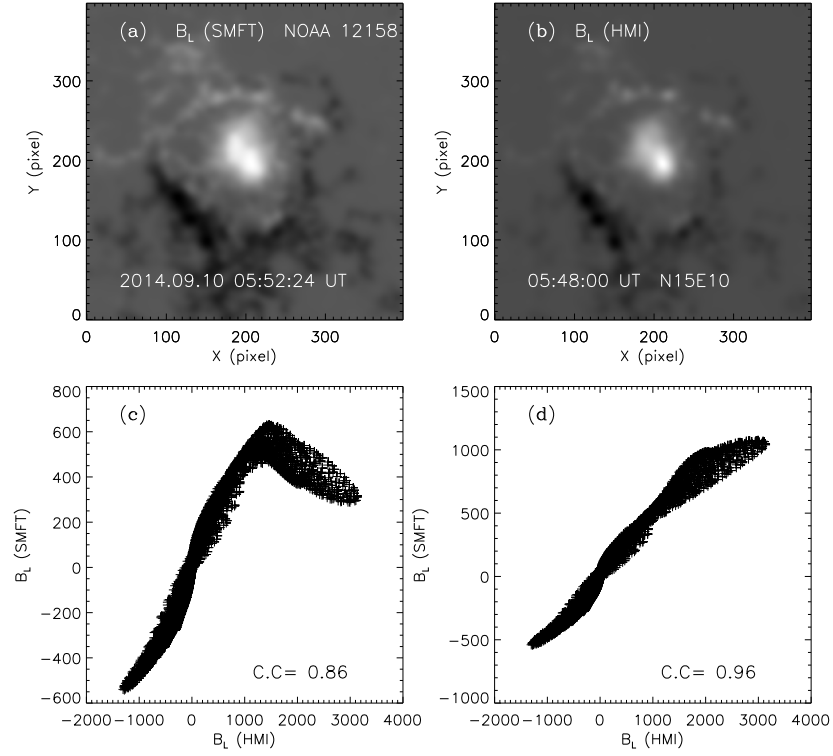The algorithm was demonstrated to be completely effective by comparing the results with HMI data for an individual

Fig. 6 Panels (a) and (b) are B_L maps of NOAA 12158 observed by SMFT and HMI, respectively. Panels (c) and (d) present the scatter plots of B_L observed by SMFT and HMI. The data taken by SMFT have saturation in (c) but no saturation in (d). C.C is the linear correlation coefficient.
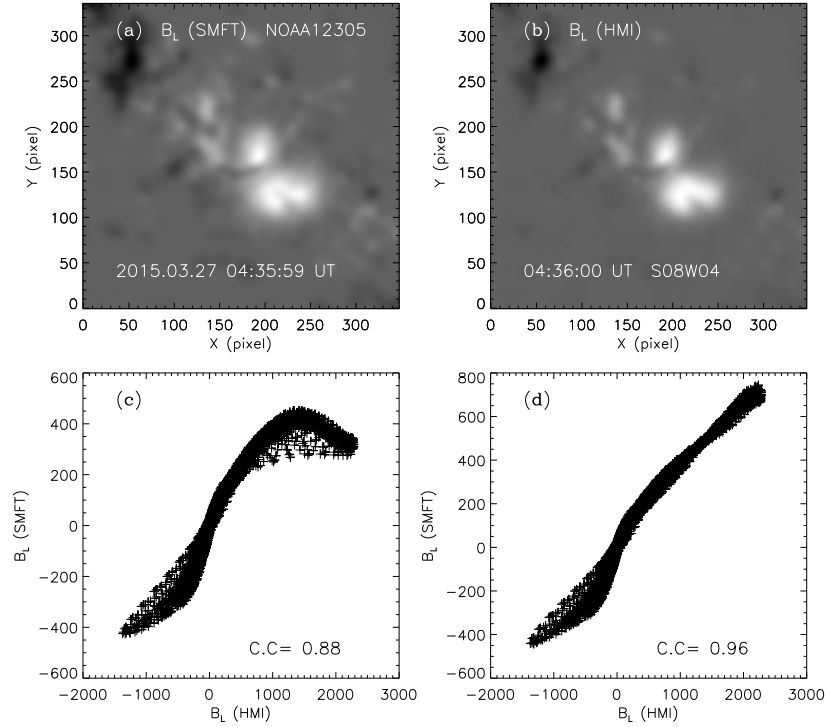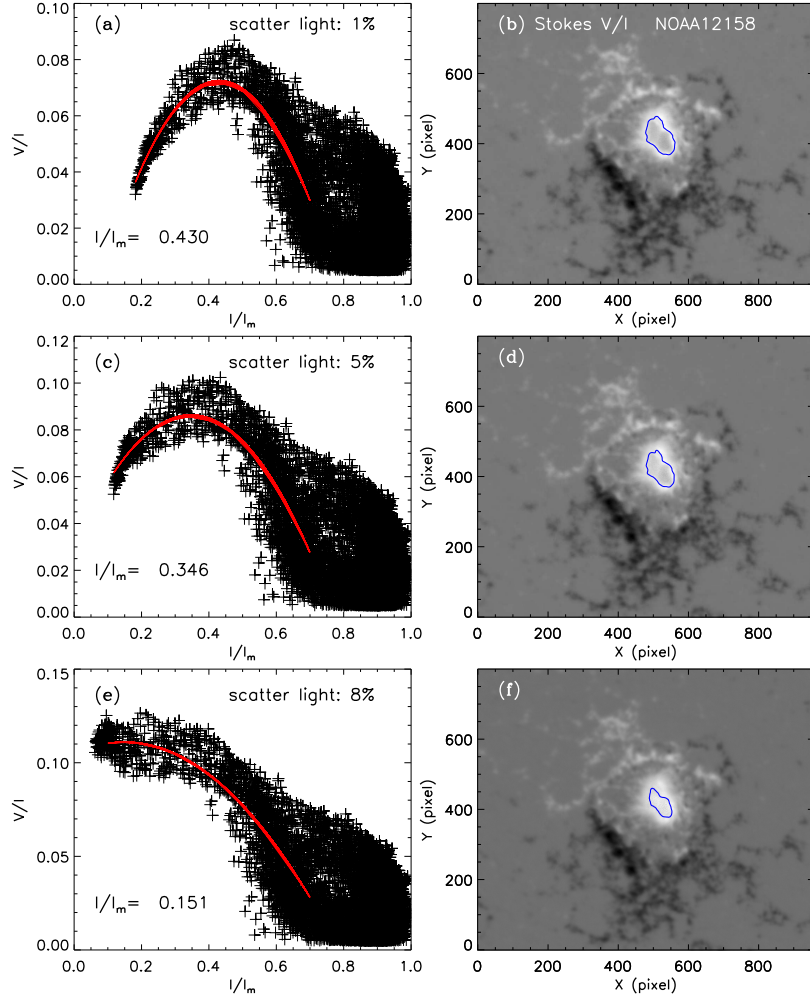

Fig. 7 Similar to Fig. 6, but for NOAA 12305.

Fig. 8 Scatter plots of $|V/I|$ vs. I/I_m and V/I maps. (a) and (b): $I_s = I_c \times 1\%$. (c) and (d): $I_s = I_c \times 5\%$. (e) and (f): $I_s = I_c \times 8\%$. In panels (a), (c) and (e), the *red line* is the second-order polynomial fit and the marked I/I_m corresponds to the apex. The *blue contours* in V/I maps represent the I/I_m apexes marked in panels (a), (c) and (e).

Table 2 Correlation Coefficient of B_L for Nine ARs Observed by SMFT and HMI

NOAA	Date	Position	C.C (before)	C.C (after)
11658	2013.01.19	S11W10	0.79	0.94
11899	2013.11.18	N06W03	0.84	0.93
11960	2014.01.25	S14E01	0.89	0.95
12027	2014.04.06	N13W01	0.85	0.95
12055	2014.05.12	N10W02	0.79	0.93
12149	2014.08.27	N10E11	0.88	0.94
12158	2014.09.10	N15E10	0.86	0.96
12305	2015.03.27	S08W04	0.88	0.96
12325	2015.04.19	N04E02	0.88	0.94

C.C (before) and C.C (after) represent the linear correlation coefficient before and after correcting magnetic saturation in B_L^{SMFT}, respectively.

AR. To check the applicability of the algorithm for a large sample, we tested it with 175 longitudinal magnetograms of 175 ARs observed in 2013 by SMFT. Magnetic saturation generally occurs in a strong field region. Considering this actual situation, we set the following restrictions:

(1) Only pixels where $|V/I| > 0.02$ and $I/I_m \leq 0.7$ are used for second-order polynomial fitting.

(2) To ensure the rationality of the fitting result, we set $I_{\min} < I_0 < 0.7$. $I_{\min}$ is the minimum value of I/I_m. If considering the 1σ error range, we can set $I_{\min} < I_{-\sigma} < I_0 < I_{+\sigma} < 0.75$.

Forty-two ARs were detected with magnetic saturation. By manual testing, the detected ARs are all correct. Only one AR with magnetic saturation was not detected by our method. So, the accurate rate of detection is $\sim$99.4%. If we adjust the I/I_m range, the above undetected AR can also be detected. It is found that magnetograms of five ARs (the total is 42) were wrong after correcting the saturation effect, which indicates that the accurate rate of

correction is $\sim 88\%$. These five ARs are either relatively small or include the projection effect. The projection effect is complex, and we need to do a further analysis of its influence on saturation.

6 CONCLUSIONS AND DISCUSSIONS

We developed an automatic detection and correction algorithm for saturation in longitudinal magnetic field observed by SMFT based on the relationship between Stokes V/I and I. It works well in comparison with HMI data and sample study. The correlation of longitudinal magnetic fields between SMFT and HMI increased significantly after correcting for saturation effect. The accuracy rate of detection and correction is $\sim 99.4\%$ and $\sim 88\%$ respectively. There is a total of 43 out of 175 ARs with saturation effect. This means 75.4% of ARs do not need to be corrected for the saturation effect.

We did not correct the scattered light when we built the I-V/I relationship. The measured polarization signals are contaminated by scattered light (I_s). E.g., if we consider the scattered light, Equation (2) will be written as follows

$$\frac{V}{I} = \frac{V_l - V_r}{V_l + V_r - 2I_s}, \qquad (5)$$
$$I = V_l + V_r - 2I_s.$$

Generally, I_s is determined at the solar limb. Here, we estimate I_s using the intensity of the quiet Sun (a certain percent of I_c). We took NOAA 12158 as an example to estimate the effect of scattered light on the method. The result is shown in Figure 8. V/I in the umbra, which increases with more scattered light, is subtracted from the observed data. When the contamination level is lower than 8% (Fig. 8(a)-(d)), the Stokes V/I vs. I/I_m curves are very similar and the areas of saturation are almost the same although the threshold of saturation is different. This aspect may be due to the normalized I/I_m being considered. The saturation area decreases and the V/I vs. I/I_m curve is close to linear when the contamination level is around 8% (Fig. 8(e) and (f)), which affirms that the measured polarized signals are likely affected more seriously by scattered light than magnetic saturation. The above estimations indicate that the proposed method will not be affected by scattered light when the contamination level is lower, and the scattered light can be corrected as a magnetic saturation effect.

One advantage of this method is that it can calculate the threshold of saturation and correct it automatically. Therefore, this method can be employed for routine longitudinal field observations. Another advantage is that the data are acquired by one instrument which avoids a systematic error caused by cross-comparison. In particular, it can be applied to correct the saturation effect in longitudinal magnetic fields in the past 30 years taken by SMFT. This method can be utilized for FMG. The disadvantage of this method is that the correction for saturation is not very accurate when the ARs are far from the disk center. This may be caused by the projection effect. We will improve the method by considering the projection effect in the future.

References

Ai, G. X., Li, W., & Zhang, H. Q. 1982, Acta Astronomica Sinica, 23, 39

Ai, G. X., & Hu, Y. F. 1986, Acta Astron. Sinica, 27, 173

Bai, X.Y., Deng, Y.Y., Teng, F., et al. 2014, MNRAS, 445, 49.

Chae, J., Moon, Y.-J., Park, Y.-D., et al. 2007, PASJ, 59, S619

Deng, Y. Y., Zhang, H. Y., Yang, J. F., et al. 2019, RAA (Research in Astronomy and Astrophysics), 19, 157

Gan, W. Q., Zhu, C., Deng, Y. Y., et al. 2019, RAA (Research in Astronomy and Astrophysics), 19, 156

Guo, J. J, Bai, X. Y., Deng, Y. Y., et al. 2020, Sol. Phys., 295, 5

Hale, G. E. 1908, ApJ, 28, 315

Kosugi, T., Matsuzaki, K., Sakao, T., et al., Sol. Phys., 243,3

Leonard, T., & Choudhary, D. P. 2008, Sol. Phys., 252, 33

Liu, Y., Nortion, A.A., & Scherrer, P.H. 2007, Sol. Phys., 241, 185

Martínez, V., & Vázquez, M. 1993, A&A, 270, 494

Moon, Y.-J., Kim, Y.-H., Park, Y.-D., et al. 2007, PASJ, 59, S625

Norton, A.A.,& Gilman, P.A. 2004, ApJ, 603, 348

Plotnikov, A., Kutsenko, A. Yang, S. B., et al. 2019, eprint arXiv:1904.07081

Schou, J., Borrero, J. M., Norton, A. A., et al. 2012, Sol. Phys., 275, 327

Su, J. T., Bai, X. Y., Chen, J., et al. 2019, RAA (Research in Astronomy and Astrophysics), 19, 161

Su, J. T., & Zhang, H. Q. 2004, ChJAA (Chin. J. Astron. Astrophys.), 4, 365

Svalgaard, L., Duvall, T.L., Jr., & Scherrer, P.H. 1978, Sol. Phys., 58, 225

Ulrich, R.K., Evans, S., Boyden, J.E., et al. 2002, Astrophys. J. Suppl. 139, 259

Wang J. X., Shi Z. X., Wang H. N., et al. 1996, ApJ, 456, 861

Zhang, H. Q. 2019, Sci. China-Phys. Mech. Astron., 62, 999601